

Identification of local extinction topology in axisymmetric bluff-body diffusion flames with a reactedness-mixture fraction presumed probability density function model

P. Koutmos^{*,1} and P. Marazioti

Department of Mechanical and Aeronautical Engineering, University of Patras, Patras, Rio, Greece

SUMMARY

The effects of finite-rate chemistry, such as partial extinctions and re-ignitions, are investigated in turbulent non-pre-mixed reacting flows stabilized in the wake of an axisymmetric bluff-body burner. A two-dimensional large-eddy simulation procedure is employed that uses a partial equilibrium/two-scalar reactedness mixture fraction probability density function (PDF) combustion sub-model, which is applied at the sub-grid scale (SGS) level. An anisotropic sub-grid eddy-viscosity and two equations for the SGS turbulence kinetic and scalar energies complete the SGS closure model. The scalar covariances required in the joint PDF formulation are obtained from an extended scale-similarity assumption between the resolved and the sub-grid fluctuations. Extinction due to strong turbulence/chemistry interactions is recognized with the help of a 'critical', locally variable, turbulent Damkohler number criterion, while transient localized extinctions and re-ignitions are treated with a Lagrangian transport equation for a reactedness progress variable. Comparisons with available experimental data suggested that the formulated approach was capable of identifying the effects of large-scale vortex structure activity, which were inherent in the reacting wake and dominant in the counterpart isothermal flows that otherwise would have been obscured if a standard time-averaged procedure had been used. Additionally, the post-extinction and re-ignition behaviour and its time-varying interaction with the large-scale structure dynamics were more appropriately addressed within the context of the present time-dependent method. Copyright © 2001 John Wiley & Sons, Ltd.

KEY WORDS: axisymmetric bluff-body stabilized flames; partial extinction and re-ignition; partial equilibrium model; large-eddy simulations; large-scale vortex structures

1. INTRODUCTION

The successful prediction of bluff-body stabilized diffusion flames is a significant issue in turbulent flame modelling technology since it provides a basis for the development of a

* Correspondence to: Department of Mechanical and Aeronautical Engineering, University of Patras, Rio 26500, Greece. Tel.: +30 61 997244; fax: +30 61 997244.

¹ E-mail: koutmos@thermo.mech.upatras.gr

calculation strategy for practical combustors [1–3]. Alongside the strong coupling between the turbulence and chemistry that results from the interaction between fuel injection and the primary recirculation, the influence of large-scale vortex structures and flow unsteadiness on entrainment, heat release and stability characteristics of bluff-body flames poses a related and equally difficult challenge for current models [4,5]. Such effects commonly arise in combustors with overall lean conditions; a situation frequently simulated by bluff-body flames operated in the air-flow dominated regime [4,6]. Flame phenomena such as ignition, extinction and re-ignition are inherently transient and interdependent with the dynamic evolution of the aerodynamic field [7,8]; therefore, suitable modelling procedures are required if such complex effects are to be properly included and evaluated within practical computational fluid dynamics (CFD) methodologies.

In this work an attempt is made to develop a mathematical model for bluff-body flames with finite-rate kinetic effects with or without the influence of large-scale structures and flow unsteadiness, while avoiding the complexity of multi-scalar treatments. As modelling requirements are significantly increased with respect to jet flames, multi-scalar approaches can sometimes be avoided and finite-rate chemistry effects can be addressed by parameterizing the local gas state in terms of a Damkohler number and by using appropriate extinction criteria [9,10]. The development of such methods relies crucially on detailed measurements of the local turbulent flame structure close to extinction [11].

The basic two-dimensional large-eddy simulation (LES) procedure developed by Koutmos [12], initially applied to the calculation of piloted jet diffusion flames with extinction effects, is adopted in the present work. In that modelling effort, a partial equilibrium/two-scalar exponential probability density function (PDF) model handled the turbulence/chemistry interactions at the sub-grid scale (SGS) level in the pre-extinction regime, while a local Damkohler number extinction criterion and a Lagrangian transport equation (Interaction by Exchange with the Mean (IEM) [1]) for a reactedness progress variable were used to treat localized extinction and the post-extinction regime. This computational model is here extended and improved in several respects. Firstly, by exploiting the basic two-scalar treatment, an adopted reactedness-mixture fraction joint PDF formulation conveniently facilitated the inclusion of the effects of turbulence interactions on the reactedness progress variable in the post-extinction regime. Secondly, a turbulent/chemical time-scale related to the local flame structure behaviour and a novel mixing asymptote gas state, as proposed by Koutmos [13], have been incorporated into the basic treatment to track consistently the post-extinction evolution of the gas state. Thirdly, an equation for the SGS scalar energy together with an extended scale-similarity assumption between resolved and SGSs now strengthens the modelling of the scalar fluctuations and allows the evaluation of the SGS moments that are required in the PDF closure both in the pre- and post-extinction regimes. All these refinements have helped enhance the basic model to meet the increased modelling requirements arising in the study of the present complex bluff-body flames.

The model here is applied to an unconfined axisymmetric bluff-body stabilised methane (CH_4) diffusion flame and its corresponding inert mixing flow that have been studied experimentally by Schefer *et al.* [4] and Masri *et al.* [11] and computationally in an ERCOFTAC Special-Interest-Group Workshop [5]. Emphasis was placed here on resolving properly the small aspect ratio fuel-jet injection orifice region. Therefore, the two-dimensional character

of the present simulations focuses on the in-plane near-wake refinement to allow the investigation of the all-important interaction of the fuel injection process with the reactive near-wake development so that any extension to three dimensions can be accomplished in a more meaningful way. The computations indicate that the time-varying large-scale vortex structures play a significant role in the development of the cold flow. Although such effects are reduced under reacting conditions, the low-energy broad band quasi-periodic motions that still influence actively the reacting wake development justify the exploitation of the present time-dependent treatment.

2. MODEL BURNER CONFIGURATION AND FLOW DETAILS

The computed burner geometry is depicted in Figure 1. Non-intrusive measurements related to this geometry have been reported by Schefer *et al.* [4], Masri *et al.* [11] and Perin *et al.* [14] for both a reactive case and its corresponding inert flow. The axisymmetric stabilizer has an outer diameter of 50 mm (D) with a concentric fuel jet of 5.4 mm diameter (d) and is surrounded by an outer tube of 100 mm in diameter (D_A) supplying the coaxial air. The containing outer tube has a lip thickness of 1 mm and ends at the bluff-body face so that an unconfined configuration results. Air of low velocity is flowing around this air tube. The computed configuration has inlet velocity settings for the fuel, air and co-flow of 21, 25 and 1 m s^{-1} respectively. The Reynolds number of the central methane fuel jet, based on the jet diameter and velocity, was maintained at 7000. At this Fuel jet/annulus Air flow Velocity Ratio (FAVR) of 0.84, the burner operates close to a borderline region between the regimes of the jet-dominated (i.e. fuel jet penetrates the primary recirculation) and annulus-dominated airflow (no jet penetration through the primary recirculation [6]). With these operational settings, the inert flow lies in the former regime and the reacting in the latter. This particular behaviour can be inferred from the reported measurements, is evidenced in the presented computations and will be discussed further in the Section 4. The specific configuration was chosen both because of its variational difficulty and because it has been explored in an ERCOFTAC workshop [5]; therefore allowing for a discussion on the performance of the present model alongside other modelling approaches.

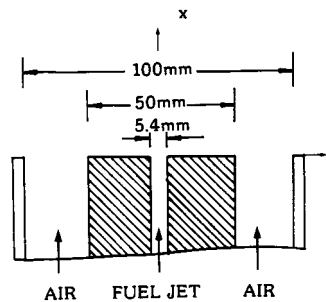


Figure 1. Flow configuration and axisymmetric bluff-body burner geometry.

3. COMPUTATIONAL MODEL FORMULATION

3.1. Aerodynamic model

The model description is derived from the formulations adopted in Koutmos [12]. Within the LES the flow variables F can be decomposed into resolvable \tilde{F} and SGS F' quantities using a Favre-weighted filter, $\tilde{F} = \overline{\rho F} / \bar{\rho}$ [15,16]. This results in the equations describing the resolvable flow quantities

$$\frac{\partial \bar{\rho}}{\partial t} + \frac{\partial \bar{\rho} \tilde{u}}{\partial x_i} = 0, \quad \frac{\partial \bar{\rho} \tilde{u}_i}{\partial t} + \frac{\partial (\bar{\rho} \tilde{u}_i \tilde{u}_j)}{\partial x_j} = - \frac{\partial \bar{p}}{\partial x_i} + \frac{\partial}{\partial x_j} \tilde{\sigma}_{ij} + \frac{\partial}{\partial x_j} \tau_{ij} + (\bar{\rho} - \rho_\infty) g_i \tag{1}$$

(ρ , μ , T and u represent density, viscosity, temperature and velocity of the gas respectively, and $i = 1, 2$ in a Cartesian system (x, y)). $\bar{p} = \bar{\rho} R_u \tilde{T} \Sigma_i Y_i / M_i$, where Y_i , M_i and R_u are the mass concentration, the molecular weight of species i and the universal gas constant respectively. $\tilde{\sigma}_{ij} = \mu (\tilde{S}_{ij} - 2/3 \tilde{S}_{kk} \delta_{ij})$, τ_{ij} are the SGS stresses and \tilde{S}_{ij} is the resolvable strain tensor. τ_{ij} is modelled as

$$\tau_{ij} = - \overline{\bar{\rho} u'_i u'_j} = \mu_{t,ij} \left(\tilde{S}_{ij} - \frac{2}{3} \tilde{S}_{kk} \delta_{ij} \right) - \frac{2}{3} \bar{\rho} \tilde{k}_s \delta_{ij}$$

where \tilde{k}_s is the SGS energy obtained from a provisional model equation of the form

$$\frac{\partial \bar{\rho} \tilde{k}_s}{\partial t} + \frac{\partial (\bar{\rho} \tilde{u}_j \tilde{k}_s)}{\partial x_j} + \frac{\partial}{\partial x_j} \left[\left(\frac{\mu}{\sigma_k} + \frac{\mu_{tjj}}{\sigma_k} \right) \frac{\partial \tilde{k}_s}{\partial x_j} \right] - \overline{\bar{\rho} u'_i u'_j} \frac{\partial \tilde{u}_i}{\partial x_j} - \frac{\mu_t}{\sigma_k} \frac{1}{\bar{\rho}^2} \frac{\partial \bar{\rho}}{\partial x_i} \frac{\partial \bar{p}}{\partial x_i} - \frac{\rho_\infty}{\bar{\rho}^2} \frac{\mu_t}{\sigma_k} \frac{\partial \bar{\rho}}{\partial x_i} g_i - \bar{\rho} C_e \frac{\tilde{k}_s^{3/2}}{L_t} \tag{2}$$

The SGS eddy viscosity could be evaluated from the SGS energy as: $\mu_t = \bar{\rho} C_k L_t \sqrt{\tilde{k}_s}$, with the SGS length scale given by $L_t = \Delta = \sqrt{\Delta x_i \Delta y_i}$, where Δ is the characteristic mesh size (filter width). Since C_k has been reported to vary significantly in various simulations, here we evaluated an anisotropic C_{kij} , following the work of Goutorbe *et al.* [17] who proposed to model the SGS fluctuations in proportion to the resolved stress tensor rather than the strain tensor. The final expression from which C_{kij} is obtained here is

$$C_{kij} = \frac{(\bar{k}_s / \bar{k}_r) \bar{R}_{ij} + (2/3) \delta_{ij} \bar{k}_s}{\Delta \sqrt{\bar{k}_s} (2 \bar{S}_{ij} - (2/3) \bar{S}_{kk} \delta_{ij})}$$

with the constraint $0.05 \leq C_{kij} \leq 0.5$. S_{ij} , R_{ij} and k_r are the resolved strain, stresses and fluctuating energy, and an overbar denotes a statistical average. Detailed tests with a range of meshes for isothermal or reacting conditions suggested that this formulation is more satisfactory and efficient than a standard Smagorinsky model or conventional $k-\epsilon$ procedures [18]. Further discussion on the impact of the SGS model on the computations is presented in Section 4.

3.2. Combustion model

3.2.1. Basic turbulence/chemistry interaction model. A simple partial equilibrium scheme was utilized by constraining the gas state with respect to a pre-specified CO₂ concentration. This two-scalar description employs the mixture fraction, f , and the CO₂ concentration, Y_{CO_2} . The reaction $CO + OH \leftrightarrow CO_2 + H$ was employed to introduce non-equilibrium effects. CO₂ formation from CO is assumed to proceed primarily via this reaction at a rate: $\dot{r}_{CO_2} = k_f Y_{CO} Y_{OH} - (k_f/k_e) Y_{CO_2} Y_H$, with k_f taken as $6.76 \times 10^{11} \exp(T/1002)$ and k_e is the equilibrium constant. Whenever the mixture strength exceeds the rich flammability limit, the composition is diluted with fuel. Within this two-scalar description the final composition is calculated from the NASA equilibrium code for given f and Y_{CO_2} values by defining Y_{CO_2} as an ‘element’. ρ , T , Y_i and \dot{r}_{CO_2} values (the gas state $Y(f, Y_{CO_2})$) are obtained in a two-dimensional library for $0 < f < 1$ and $0 < Y_{CO_2} < Y_{CO_2, \max}$. The evolution of the passive, f , and the reactive, Y_{CO_2} variables, is calculated from the equations

$$\frac{\partial(\bar{\rho}\tilde{f})}{\partial t} + \frac{\partial}{\partial x_j} (\bar{\rho}\tilde{u}_j\tilde{f}) = \frac{\partial}{\partial x_j} \left[\frac{\mu}{Sc} \frac{\partial\tilde{f}}{\partial x_j} - \overline{\rho u'_j f'} \right] \tag{3}$$

$$\frac{\partial(\bar{\rho}\tilde{Y}_{CO_2})}{\partial t} + \frac{\partial}{\partial x_j} (\bar{\rho}\tilde{u}_j\tilde{Y}_{CO_2}) = \frac{\partial}{\partial x_j} \left[\frac{\mu}{Sc} \frac{\partial\tilde{Y}_{CO_2}}{\partial x_j} - \overline{\rho u'_j Y'_{CO_2}} \right] + \bar{\rho}\tilde{r}_{CO_2} \tag{4}$$

with $\overline{u'_j f'}$ and $\overline{u'_j Y'_{CO_2}}$ obtained from the anisotropic SGS viscosity as

$$-\overline{\rho u'_j f'} = \frac{\mu_{tj}}{Sc_t} \frac{\partial\tilde{f}}{\partial x_j}, \quad -\overline{\rho u'_j Y'_{CO_2}} = \frac{\mu_{tj}}{Sc_t} \frac{\partial\tilde{Y}_{CO_2}}{\partial x_j}$$

An exponential PDF of the form

$$P(f^*, Y_{CO_2}^*) = \exp(a_1 + a_2 f^* + a_3 Y_{CO_2}^* + a_4 f^{*2} + a_5 Y_{CO_2}^{*2} + a_6 f^* Y_{CO_2}^*)$$

is constructed from the normalized concentrations f^* and $Y_{CO_2}^*$, which transform the f and Y_{CO_2} space into a square area suitable for integration and is calculated through the coefficients (a_1 – a_6), which depend on the local SGS moments $\overline{f'^2}$, $\overline{Y'_{CO_2}{}^2}$ and $\overline{f' Y'_{CO_2}}$. A discussion on the benefits of exploiting a PDF within the context of the LES has been provided by Jimenez *et al.* [19].

Within the present work, the SGS scalar fluctuation energy, $k_{fs} = \frac{1}{2}\overline{f'^2}$, is obtained from a model equation of the following form:

$$\frac{\partial(\bar{\rho}\tilde{k}_{fs})}{\partial t} + \frac{\partial(\bar{\rho}\tilde{u}_j\tilde{k}_{fs})}{\partial x_j} = \frac{\partial}{\partial x_j} \left[\left(\frac{\mu}{Sc} + \frac{\mu_{tj}}{Sc_t} \right) \frac{\partial\tilde{k}_{fs}}{\partial x_j} \right] + \frac{1}{2} C_1 \frac{\mu_t}{Sc_t} \frac{\partial\tilde{f}}{\partial x_j} \frac{\partial\tilde{f}}{\partial x_j} - \rho C_2 \frac{1}{\tau_t} \tilde{k}_{fs} \tag{5}$$

with $C_1 = C_2 = 2.0$ and $\tau_t = L_t/\sqrt{\tilde{k}_s}$. The remaining moments required in the PDF closure are modelled in line with the extended scale similarity assumption as follows: $\tilde{Y'_{CO_2}{}^2} = (\tilde{k}_{fs}/\tilde{k}_{fr})R_{CO_2}$, $\tilde{f' Y'_{CO_2}} = (\tilde{k}_{fs}/\tilde{k}_{fr})R_{fCO_2}$, where \tilde{k}_{fr} is the resolved scalar fluctuation energy and R_{CO_2} , R_{fCO_2} are

the resolved fluctuations. The PDF constants are then determined from normalization conditions and expressions for the moments resulting from integration of the functional PDF form. The Favre-resolved gas state vector, \tilde{Y} (i.e. ρ , T , Y_i , etc.), is evaluated by integration at each time-step as

$$\tilde{Y} = \frac{1}{\bar{\rho}} \int YJ\rho P(f^*, Y_{\text{CO}_2}^*) df^* dY_{\text{CO}_2}^*$$

where J is the Jacobian of the transformation.

3.2.2. Extinction/re-ignition model. The modelling of finite-rate chemistry effects, such as localized extinctions and re-ignitions, is based on the analysis of Koutmos [13]. Local extinction is predicted when the local Damkohler, Da_i , defined as the ratio of the turbulent time scale, $\tau_\lambda = 3.88$ (τ_k is the Kolmogorov time) to the chemical time scale, τ_{ch} , is below a local 'critical' Damkohler, Da_{cr} , which is a function of position and local conditions. The local quenching criterion then reads

$$\lambda = \frac{Da_i}{Da_{\text{cr}}} = \frac{[\tau_\lambda/\tau_{\text{ch}}]}{\left[\frac{\Sigma f}{\sqrt{2}\Delta f_{\text{R}}} Re^{1/4} \right]} \leq 1 \quad (6)$$

$\Sigma f = \varepsilon_f^{1/2}(\nu/\varepsilon)^{1/4}$ is the Gibson scalar scale where ε , ε_f are the dissipation rates of the turbulence kinetic and scalar energies. A variable 'effective' reaction zone width in mixture fraction space, Δf_{R} , is defined as $\Delta f_{\text{R}} = \Delta f_{\text{RS}} = f_{\text{R}} - f_{\text{L}}$ for $f_{\text{L}} \leq f \leq f_{\text{R}}$, $\Delta f_{\text{R}} = \Delta f_{\text{RS}} + f - f_{\text{R}}$ for $f > f_{\text{R}}$ and $\Delta f_{\text{R}} = \Delta f_{\text{RS}} + f_{\text{L}} - f$ for $f < f_{\text{L}}$, where $f_{\text{L,R}}$ are the reach and lean flammability limits respectively. The chemical time scale above is taken from the partial equilibrium model as $\tau_{\text{ch}} = 1/[\dot{r}_{\text{CO}_2}(f^*, Y_{\text{CO}_2}^* = 0)]$ for $f_{\text{L}} \leq f \leq f_{\text{R}}$, $\tau_{\text{ch}} = 1/[\dot{r}_{\text{CO}_2}(f_{\text{L}}^*, Y_{\text{CO}_2}^* = 0)]$ for $f < f_{\text{L}}$ and $\tau_{\text{ch}} = 1/[\dot{r}_{\text{CO}_2}(f_{\text{R}}^*, Y_{\text{CO}_2}^* = 0)]$ for $f > f_{\text{R}}$. The Favre-resolved τ_{ch} value, determined by integration with the PDF, is used in the above criterion. Opposite to previously employed extinction criteria (e.g. Obounou *et al.* [9] and Gran *et al.* [10]), where the local Damkohler was compared with an arbitrarily chosen critical level (e.g. $Da \leq 1$), the present formulated criterion allows a wider flexibility by relating the local Damkohler to *local* turbulent scalar mixing and chemical parameters that vary with time, position and local flame structure conditions.

Whenever Equation (6) holds true, extinction is predicted and the chemical source in Equation (4) is set to zero. The post-extinction regime and the probable re-ignition behaviour of the locally extinguished location are modelled by defining the following gas states in mixture fraction space: (a) $Y_{\text{E}} = Y_{\text{E}}(f^*, Y_{\text{CO}_2}^*)$, representing undisturbed burning at partial equilibrium (when $\lambda > 1$). The Favre-resolved gas state at each time step is then determined as described in Section 3.2.1. (b) $Y_{\text{O}} = Y_{\text{O}}(f^*, Y_{\text{CO}_2}^* = 0)$, representing the lower equilibrium bound (i.e. the high strain rate limit state within the partial equilibrium treatment). (c) A 'limit' mixing asymptote state, Y_{M} , defined as described below. (d) $Y_{\text{I}} = Y_{\text{I}}(f^*)$, representing inert mixing between fuel and air. (e) Any intermediate state, Y_{Q} , between O and I, representing the post-extinction transition from undisturbed burning to inert mixing and vice versa. The state Y_{Q} is a function of the mixture fraction and of the local value of the reactedness, B , which is defined as $B = (Y - Y_{\text{I}})/(Y_{\text{O}} - Y_{\text{I}})$.

From a detailed analysis of the flame structure data reported by Masri *et al.* [11] on piloted methane jet diffusion flames, Koutmos [13] demonstrated that the distributions of the time-averaged λ parameter as given by Equation (6), when plotted against mixture fraction at various axial flame positions and for a range of fuel jet velocities close to extinction, follow the curves displayed in Figure 2. It was observed that when $\lambda < 1$ over the whole extent of the reaction zone width, Δf_{RS} , completely extinguished flame conditions result. It was further shown therein that the measured extinguished samples lie on a temperature (or species) asymptote, Y_M (line EME', Figure 2 (inset)), that (a) intersects the rich equilibrium branch at an f position coincident with the rich cross-over position of λ above 1 supporting the above criterion, and (b) the reactedness, B_M , of this temperature distribution (or gas state, line EME', Figure 2 (inset)) is well described by an equation of the form: $B_M = B_O \exp[-G(\lambda) * Da_{cr}]$. This result was arrived at [13] by using the IEM equation [1] to track the evolution of an extinguished 'particle' from the high strain partial equilibrium state O toward the mixing line I, i.e. $dB/dt = (B_I - B)/\tau_e = -B/\tau_e$ (with $B_I \equiv 0$). Here a novel turbulent/chemical exchange time scale, τ_e , is adopted and defined as $L_{R,t}/\sqrt{k_s}$, where $L_{R,t} = (\sqrt{2}\Delta f_R/\Sigma_f)Re_t^{-3/4} * L_t$ is the physical reaction zone width [11] and it can be readily shown that the following relationship holds: $\tau_e = \tau_\lambda/Da_{cr}$. By integrating the above IEM equation over an eddy turnover time, τ_λ , the mixing asymptote state Y_M (line EME', Figure 2) can be determined for a range of compositions and mixing conditions. The parameter $G = 1 + \lambda(1 - \lambda)$ was incorporated to introduce the 'effective' decrease of the reaction zone thickness, $L_{R,t}$, in the transition from the high

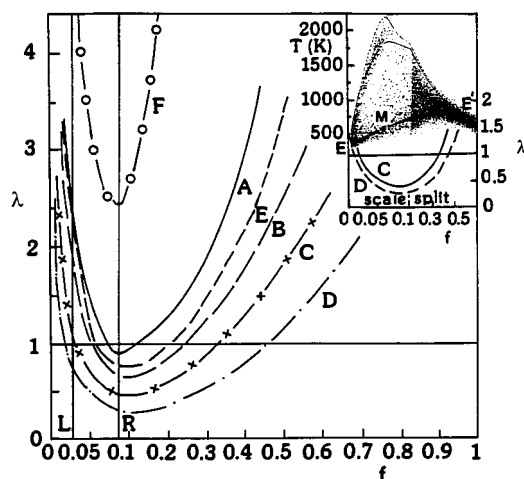


Figure 2. Distributions of the time-averaged λ values, Equation (6), for a range of methane jet flame velocities and positions [experimental data from the piloted jet flame configurations of Masri *et al.* [11]; (A) $u_j = 36 \text{ m s}^{-1}$, $x/D_j = 20$; (B) $u_j = 41 \text{ m s}^{-1}$, $x/D_j = 20$; (C) $u_j = 48 \text{ m s}^{-1}$, $x/D_j = 20$; (D) $u_j = 55 \text{ m s}^{-1}$, $x/D_j = 20$; (E) $u_j = 55 \text{ m s}^{-1}$, $x/D_j = 30$; (F) $u_j = 55 \text{ m s}^{-1}$, $x/D_j = 50$]. Figure inset: definition of mixing asymptote state Y_M and comparisons of the predictions of Koutmos [13], line EME', with the measured temperature scatterplots for flames C and D.

strain rate limit state O to state I and vice versa. Additionally, a flame thickness parameter, $\gamma = (\Delta f_{RS}/f_S) - 1$, is introduced to account for the rate of this decrease in mixture fraction space; i.e. $\gamma \approx 0$ for thin zones (e.g. CH₄), denoting the more abrupt reduction of $L_{R,t}$ in this case, whilst $\gamma \approx 0.4$ for fuels with wider zones, e.g. CO/H₂/N₂ mixtures.

Within the present treatment, the mean value \bar{Y}_O can be obtained by convoluting with the local exponential two-dimensional PDF: $\bar{Y}_O = (1/\bar{\rho}) \iint Y_O \rho P(\tilde{f}, \tilde{B}) d\tilde{f} d\tilde{B}$. The values of \tilde{B} and \tilde{B}'^2 required to close the PDF formulation are evaluated as described below. The Favre-resolved reactedness, \tilde{B} , is calculated from the following model transport equation:

$$\frac{\partial(\rho\tilde{B})}{\partial t} + \frac{\partial(\bar{\rho}\tilde{u}_j\tilde{B})}{\partial x_j} = S_B \quad (7)$$

while its SGS fluctuations, \tilde{B}'^2 and $\bar{f}'\tilde{B}'$ required to close the reactedness-mixture fraction PDF treatment in the post-extinction regime are obtained by invoking the extended scale-similarity assumption of Sections 3.2.1 and 3.2.2. With the initial value of \tilde{B} set by the partial equilibrium, S_B is set to zero if no extinction has occurred, while $S_B = (B_M - \tilde{B})/\tau_e$ after extinction has been detected. Equation (7) integrates in a Lagrangian sense the history of the gas state assuming that post-extinction mixing of the partial equilibrium products is represented by a deterministic relaxation to the inert value. One implication of the above formulation is that the broadening of the reaction zone in mixture fraction space, e.g. due to dilution of fuel, is accounted for and this is an aspect that has been stressed in a number of works [11] in relation to the bimodal or monomodal behaviour of the reactive scalar PDF close to extinction. According to the present variable reaction zone thickness (Δf_R) formulation, the exchange time τ_e in the source of Equation (7) for lean CH₄ compositions, which have a Δf_R of 0.055 (and $Da_{cr} \sim 1/\Delta f_R$), is much less than half the eddy time τ_λ (since $\tau_e \sim \tau_\lambda(1/Da_{cr}) \sim \tau_\lambda\Delta f_R$). Integration of Equation (7) over a time step of the order of τ_λ will therefore result in either fully burned or extinguished states recovering the experimentally observed bimodal behaviour of the reactedness PDF. For rich CH₄ compositions or in fuels with much broader reaction zones, e.g. air-diluted CH₄ fuels, Δf_R is almost ten times the above H/C values and τ_e attains values almost ten times those of lean CH₄ conditions. The above formulation is therefore likely to reproduce the gradual shift of measured scatter-points to extinction for such fuels and compositions while at the same time permits the treatment of the interaction between the local turbulence and the transient extinction/re-ignition gas state evolutions.

Re-ignition is allowed when (a) the time scale criterion is inoperative and (b) the cumulative probability of finding a flammable mixture at this location, defined as $P_F = \int_{f_L}^{f_R} P(f^*) df^*$, is greater than 0.75. If the above two conditions prevail then the source term in Equation (7) is set to $(B_O - \tilde{B})/\tau_{id}$, where τ_{id} is a mixing-dependent chemical ignition delay time. The procedure of Obounou *et al.* [9] is closely followed for the determination of τ_{id} . Briefly, the IEM equations for species and temperature are solved over a range of f , Y_{O_2} and mixing time values for a single-step CH₄ oxidation producing a two-dimensional library $\tau_{id} = \tau_{id}(\tilde{f}, \tilde{Y}_{O_2})$, which is subsequently used in the calculation. Further details on this may be found in Obounou *et al.* [9].

3.3. Numerical details

The filtered equations have been solved by a finite volume method employing the explicit finite difference scheme QUICKEST [20]. The equations have been discretized in a staggered mesh using an explicit quadratic Leith-type of temporal discretization [21]. The solution proceeds in three steps. In the predictor step, the momentum equation is time-advanced without the pressure term. Subsequently, the provisional velocity field is projected onto a divergence-free space by introducing a pressure correction variable that is obtained from the Poisson equation, which is solved by a conjugate gradient method with incomplete Cholesky preconditioning to obtain the pressure. The pressure correction variable is then used to correct the previously obtained provisional velocity field. The scheme has the attribute of third-order upwind differencing for the convective terms, which, in principle, are of high accuracy and low dissipation on carefully stretched grids and have been used in various works (e.g. Davis *et al.* [21]).

Both the small time-step chosen (10^{-5} s) and the carefully selected mesh spacings helped reduce the numerical discretization errors. The axisymmetric computational domain extended from $1.0D$ upstream to $27D$ downstream of the bluff-body face. Four meshes were tested in the grid refinement study comprising 155×131 , 225×183 , 271×221 and 341×285 (x, r) grid nodes. Between the third and the fourth grid level deviations in the first moment statistics were of the order of 2.2 per cent while the disagreement in the higher order statistics increased to about 6.4 per cent. The third grid was used for the presented computations while further discussion on the effects of the mesh density are provided in Section 4 both for the isothermal and the reacting performance. Although a three-dimensional simulation would have been more preferable within the LES context, the two-dimensional procedure employed here was chosen as a tool for the investigation into the applicability of such a combined turbulence/two-scalar chemistry closure methodology for the study of reacting flows within complex flow/geometry configurations of practical importance. The low aspect ratio concentric fuel jet used (fuel-jet injection orifice:bluff-body stabilizer:coaxial air-tube diameter ratio = 1:9.26:18.5) necessitated increased mesh resolution on the axial plane to resolve adequately the near-wake orifice region. Furthermore, the use of the present axisymmetric mesh system would entail a prohibitive mesh density near the orifice axis within the context of a full three-dimensional treatment [22], something that could have rendered impractical the exploitation and investigation of the adopted combined two-scalar partial equilibrium/post-extinction/re-ignition turbulence/chemistry treatment. The extension of the basic method to the computation of the present axisymmetric recirculating reacting flows is also supported by its previous successful use in predicting the slender bluff-body stabilized propane diffusion flames reported in Koutmos *et al.* [18]. In such complex flow geometry configurations, the use of a two-dimensional reactive LES with two-scalar chemistry resolves some important features of the large-scale structure field, while the three-dimensional small scale turbulence is, to a large extent, accounted for by the sub-grid PDF closure [19]. Extension to three dimensions can be accomplished at an additional cost once the combined aerodynamic/combustion modelling procedure has been thoroughly appraised.

The non-slip boundary condition for the grid-scale velocity was applied at the solid boundaries with a Van Driest damping function [23] to account for bluff-body wall proximity.

Neumann boundary conditions were employed for the pressure Poisson equation [24]. Inflow conditions were specified where possible from reported measurements, but also from standard $k-\varepsilon/\beta$ -PDF computations that provided fully developed conditions at the inlet. At the outlet the simple convective boundary condition $\partial\tilde{\Phi}/\partial t + U_0(\partial\tilde{\Phi}/\partial x) = 0$ found to work satisfactorily for the isothermal counterpart flows was employed in the reacting simulations as well. After an initial transient of $50t_0$ ($t_0 = D/U_0$) flow statistics were computed over approximately $150t_0$. The run times on a dedicated HP 735 Risc System were about 3.5 h per shedding cycle in the isothermal case and 90 CPU h for the reacting flow.

4. RESULTS AND DISCUSSION

Results from the simulations of the isothermal and reacting flows are presented in the form of time-mean data and statistical quantities while comparisons are made with the available experimental information and the calculations reported by Nau *et al.* [25], which were performed with a time-averaged finite volume/Monte Carlo transported PDF method. First the unignited wake will be presented to highlight differences between reacting and inert flows and enable a discussion on the effect of combustion on the predicted wake aerodynamics in a step by step development and appraisal of the complete model.

The overall computed cold flow development is displayed in Figure 3 in the form of a time-averaged streakline plot. At this injection ratio (FAVR = 0.84) the stagnation of the jet is predicted to occur within the primary recirculation and the mixing pattern produced by the computational flow visualization is very close to the experimentally determined flow topology reported in Schefer *et al.* [4]. The injected fuel is opposed by the primary backflow and, in part, recirculates adjacent to the bluff-body face and, in part, supplies the flanks of the primary vortex with unignited fuel creating a system of two toroidal counter-rotating vortices.

Detailed comparisons between measured and computed distributions of mean velocity, turbulence kinetic energy, mixture fraction and its variance along the axis of symmetry are depicted in Figure 4. In the axial velocity profile, Figure 4(a), the annulus airflow stagnation position and the jet impingement and deflection point are underestimated by 4 and 10 per cent

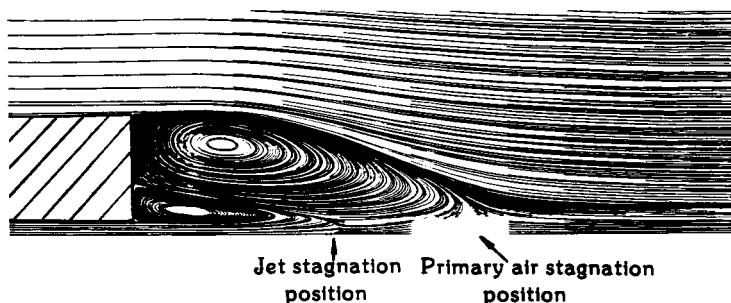


Figure 3. Computed time-averaged streakline plot for isothermal burner operation (FAVR = 0.84).

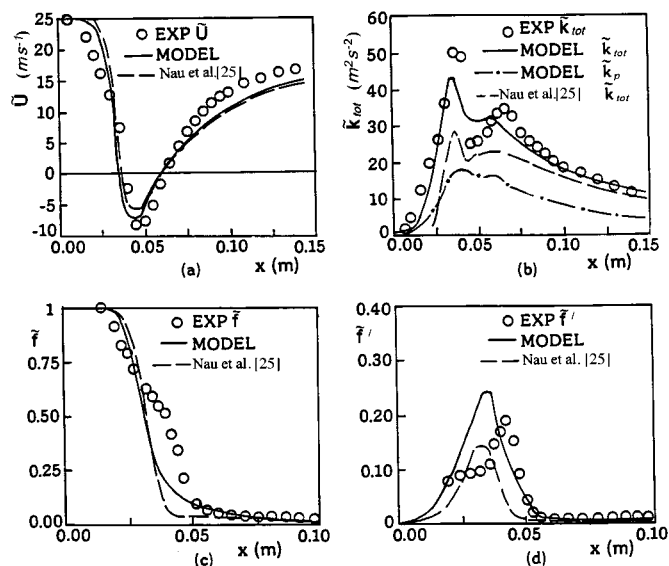


Figure 4. Comparisons of measured and calculated centre-line distributions for the isothermal flow of (a) mean axial velocity, (b) turbulent kinetic energy, (c) mean mixture fraction (inert), (d) mixture fraction fluctuations (inert).

respectively. A slight improvement is observed in the predicted maximum backflow velocities on the axis with respect to the time-averaged computations reported in Nau *et al.* [25], while the downstream wake replenishment is followed well. The two inversion points on the centreline axial velocity distribution are responsible for the two peaks in the total kinetic energy profile shown in Figure 4(b). The present method reproduces well their location but underestimates their levels by 20 per cent.

From the point of view of the present contribution it is significant to analyse the time-varying behaviour of this flow configuration that may well be obscured if a standard time-averaged computation is employed. For instance, analysis of the present simulation data revealed a distinct frequency in the spectral distributions that, most probably, is associated with the existence of organized eddy structures. In Figure 5 the computed V velocity power spectra at $x/D = 3$ on the axis show a well-defined frequency peak at about 320 Hz and verify the unsteady character of this jet/wake system. The predicted frequency is close to the experimentally determined vortex shedding frequency of 300 Hz for this configuration [4]. The time-averaged turbulence energy distribution of Figure 4(b), therefore, contains both periodic and (purely) stochastic contributions. The periodic component was here extracted by appropriate phase averaging and is plotted in Figure 4(b). This contribution is evidently sizeable near the vortex formation region diminishing gradually at downstream positions. In line with the momentum field, the computed centreline gradient of the mean mixture fraction (Figure 4(c)) and its peak fluctuation levels (Figure 4(d)) show definite improvements with respect to the

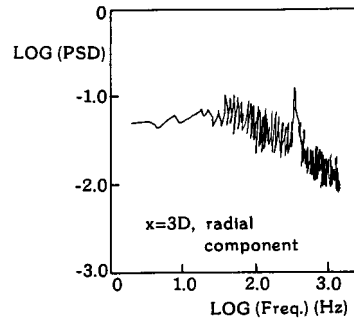


Figure 5. Computed unnormalized Power Spectral Density (PSD) for the radial component, $x/D = 3$, $r/D = 0$ ($D =$ axisymmetric bluff-body diameter).

time-averaged computations of Nau *et al.* [25]. This improved agreement in the prediction of the mixture fraction gradient (Figure 4(c)) and of its fluctuations is attributed to the exploitation of Equation (5) and to the appropriate representation of the periodic content of the turbulence energy (Figure 4(b)). The overall accord depicted for the mixing field lends support to the adopted aerodynamic and turbulent SGS models and allows for an assessment of the combustion sub-model.

Turning next to the ignited configuration, the reactive flow pattern can be better visualized in the time-averaged streaklines of Figure 6. In both measurements [4,14] and simulations, the two counter-rotating toroidal recirculation regions are again maintained in the near wake. Due to heat release and expansion the central jet induced recirculation (retaining the same FAVR value as in the cold flow) is now significantly enlarged and strong enough to reach deep into the aft end of the primary recirculation almost penetrating through it. Examining the computed centreline mean axial velocity profile in Figure 7(a), it is clear that now there is no flow inversion on the axis but merely one velocity minimum at about $x/D = 1.4$. The length of the reactive flow recirculation (measured off-axis) is overpredicted by 10 per cent. The corresponding total turbulence energy development is qualitatively more similar to the inert flow, but interestingly its periodic content is now severely reduced within the primary vortex system and increases only beyond $x/D = 2$ in an opposite fashion to the cold flow distribution.

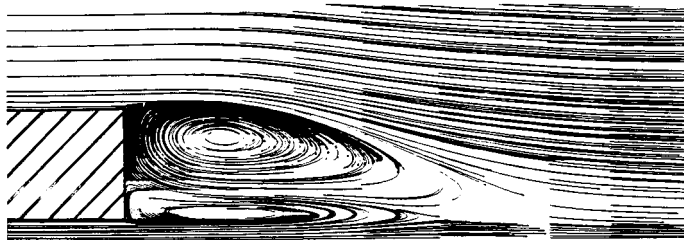


Figure 6. Computed time-averaged streakline plot for reacting burner configuration (FAVR = 0.84).

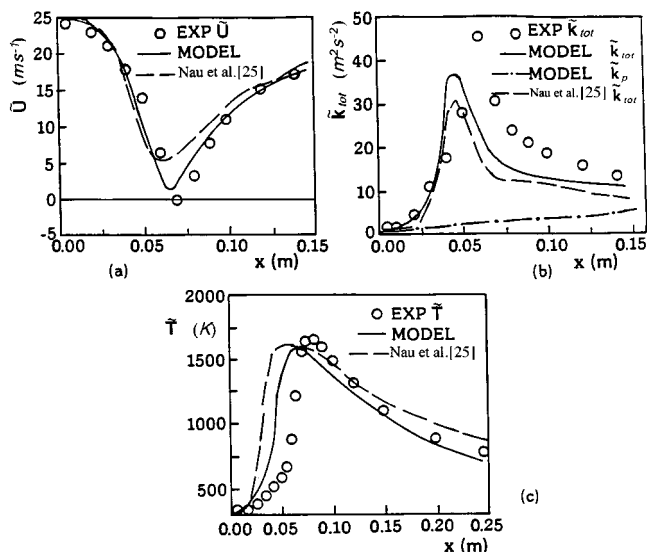


Figure 7. Comparisons of measured and calculated centre-line distributions in reacting flow of (a) mean axial velocity, (b) turbulent kinetic energy, (c) mean temperature.

Apart from the detailed comparisons with experimental data it is also important to elucidate the advantages of the employed SGS model as well as to assess the effectiveness of the adopted grid refinement level. A systematic investigation was, therefore, undertaken and results for both the isothermal and the reacting flow are depicted in Figure 8. The comparisons between measurements and computations with the two finer grids (Grid 1 = 271×221 and Grid 2 = 341×285) indicated that this additional increase in the density of the standard mesh, which is employed for the results discussed herein, merely produces a marginal improvement in the near orifice region while it has a minimal impact on the developing momentum (Figure 8(a) and (c)) and mixing (Figure 8(b) and (d)) wake fields under both inert and reactive conditions. On the other hand, the omission of the SGS model (retaining the basic Grid 1) revealed a more drastic effect on the quality of the simulations. Under isothermal conditions this caused an overestimation of the resolved fluctuations and a consequent shorter recirculation region (Figure 8(a)) together with abnormally elevated turbulence levels (Figure 8(b)). With reaction the lack of the sub-grid diffusion contribution produced an overpenetration of the fuel jet and a faster wake replenishment. Overall the use of the SGS model is deemed clearly beneficial for the present two-dimensional runs but a fuller appraisal would entail three-dimensional simulations that represent properly the mechanism of vortex stretching.

The above flame development should be seen in conjunction with the time-varying quality of the reacting flow. It has been visualized [4], postulated [6] and confirmed by detailed measurements [26] that bluff-body flames of this type exhibit unsteady partial extinctions and re-ignitions that have been interpreted [6] as stretched flame pockets (also referred to as flame

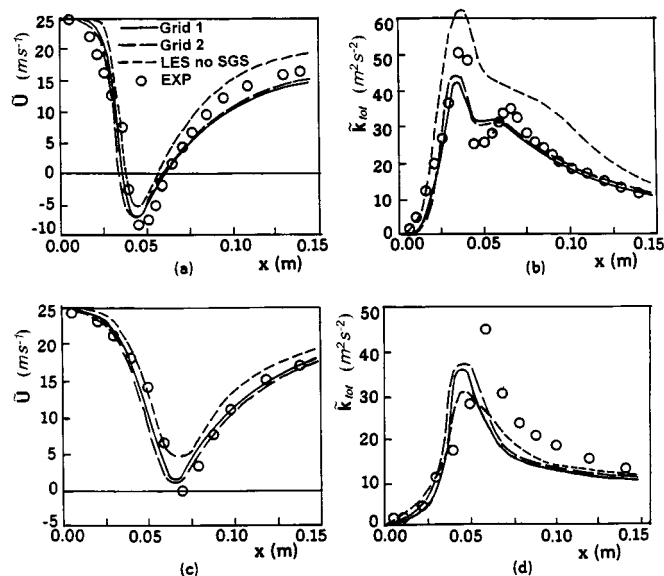


Figure 8. Grid refinement studies and contribution of subgrid model: (a) mean axial velocity, isothermal flow; (b) turbulence kinetic energy, isothermal flow; (c) mean axial velocity, reactive flow; (d) turbulence kinetic energy, reactive flow (Grid 1 = 271×221 and Grid 2 = 341×285 , LES without SGS model were performed on Grid 1).

‘turbules’) that intermittently escape from the recirculation zone and are transported further downstream though locally extinguished zones.

Examining the spatial distributions of the predicted mean extinction parameter, λ (Figure 9), we observe two regions at about $x/D = 2.2$, where local extinction and re-ignition effects are significant (i.e. where $\lambda \leq 1$). The depicted λ patterns are corroborated by the experimental evidence of Neveu *et al.* [26] on the topology of local extinction zones in flames of similar type. Here the computed low λ area in the vicinity of the symmetry axis exhibits a variable disposition with time (Figure 9(a)–(c)). The transient evolution of the gas reactivity can be verified by inspecting the joint statistics between reactive scalars and mixture fraction; the present time-dependent method is capable of providing such useful information. A T – f scatterplot, collected at $x/D = 3$, is shown in Figure 10(a). The post-extinction treatment produces bimodal reactedness PDFs with predicted states lying either within the partial equilibrium zone or (more frequently) in the vicinity of the post-extinction mixing asymptote (the Y_M state line as defined in Section 3.2.2) with only a few transitional points scattered in between. This picture is similar to the bimodal reactedness PDFs measured in simpler piloted methane jet diffusion flames with extensive regions of localised extinction [11]. The above results are consistent with calculated scatterplots for the ‘critical’ Damkohler, Da_{cr} , and the extinction parameter, λ , plotted against mixture fraction at the same station (Figure 10(b)). The deduced λ scatterpoints lie below, above or close to the limit value of one signifying the transient occurrence of the predicted localized extinctions and re-ignitions.

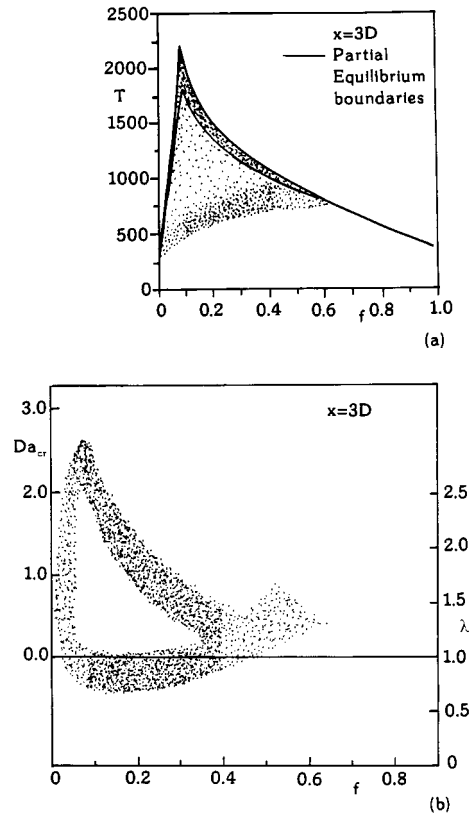


Figure 10. Computed joint PDF scatterplots ($x/D = 3$) of (a) temperature vs mixture fraction and (b) λ and Da_{cr} vs mixture fraction.

primary recirculation and their reoccurrence at downstream locations has also been discussed by Roquemore *et al.* [6] for their axisymmetric bluff-body stabilised flames.

The use of a standard time-averaged procedure is therefore questionable as it would have obscured many intrinsic features of this flame and possibly misled the interpretation of the computed results. Any improvements produced by the present simulations with respect to previous calculations, e.g. in the temperature profile (Figure 7(c)) both in the near (up to $x < 50$ mm) and in the downstream wake ($x > 120$ mm) should be seen as the result of the exploitation of the time-dependent treatment in conjunction with the extinction/re-ignition combustion sub-model. One should obviously be cautioned that the present approach is expected to be clearly inferior to a multi-step chemistry Monte Carlo PDF procedure [1,2,25]) as far as the detailed prediction of pollutant species is concerned. Since the present reactedness treatment relies on the partial equilibrium initial condition of the gas state, $Y_O = Y_O(f^*, Y_{CO_2}^* = 0)$, the inefficiencies of the partial equilibrium model are unavoidably inherent

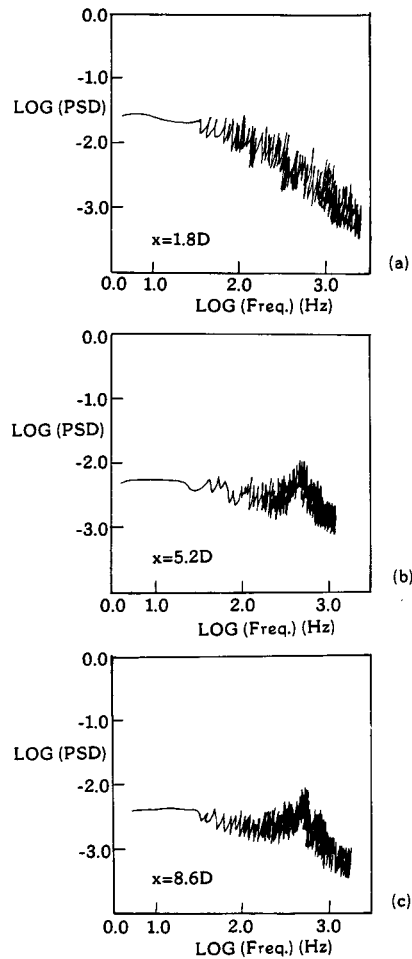


Figure 11. Computed unnormalized Power Spectral Density (PSD) for the radial component: (a) $x/D = 1.8$, (b) $x/D = 5.2$, (c) $x/D = 8.6$.

in the present procedure. However, for bluff-body flame configurations operated well in the air-dominated regime or close to global extinction conditions, where the effects of organized motions become more pronounced, the usefulness of an LES methodology against more conventional treatments is expected to increase.

The use of the B equation in the extinction treatment is similar to the coalescence/dispersion model employed in Monte Carlo/PDF calculations [2,25]. Through the post-extinction 'turbulent/chemical' exchange time scale, τ_e , the effects of combustion on mixing are now modelled and implemented, at least to first order, within the simple chemistry employed so far. A possible extension would be to involve the solution of more B equations with appropriate

source terms for selected reactive scalars. Although the present method possibly offers a simpler alternative for introducing effects of finite-rate chemistry, such as extinctions and re-ignitions, one should be clearly reminded of the potential and benefits of a tractable ‘multi-step chemistry’ computational scheme (e.g. Borghi *et al.* [1], Tolpadi *et al.* [2], Nau *et al.* [25]) when a detailed knowledge of combustor emissions is desired. The development of such a flexible scheme in combination with a time-accurate procedure would undoubtedly provide a powerful tool for the study of complex turbulent reacting flows as studied here.

5. SUMMARY

Axisymmetric bluff-body diffusion flames and their unignited counterpart inert flows were computed with a two-dimensional LES approach utilizing a partial equilibrium/two-scalar exponential PDF combustion sub-model and two equations for the turbulence kinetic and scalar energies employed at the SGS level. The effects of strong turbulence/chemistry interactions were addressed by coupling the basic partial equilibrium description to an extinction/re-ignition regime while preserving the two-scalar character of the basic method. With an appropriate turbulent extinction criterion and treatment of the transient evolution of the quenched and re-ignited gas states via a Lagrangian reactedness equation, many significant features and interactions between the large-scale vortex dynamics and the local flame structure were recovered in the simulated reactive wake. The present method gains in popularity from the fact that such dynamic interactions apparently seem to be common in many other bluff-body stabilized flame configurations. Therefore its use, through further tests, refinements or extensions could prove useful for the characterization and control (passive or active) of combustor flows with inherent time-dependent behaviour.

APPENDIX A. NOMENCLATURE

B	reactedness progress variable
C_{kij}	SGS model constants
d	fuel-jet injection orifice diameter in bluff-body
D	axisymmetric bluff-body diameter
Da	Damkohler number
f/f^*	mixture fraction/normalized
$f_{L,R}$	Lean/rich mixture fraction flammability limits
FAR/FAVR	Fuel–air/fuel–air velocity ratios
IEM	interaction by exchange with the mean model
J	Jacobian of transformation (two-scalar PDF)
k_f, k_e	forward reaction rate/equilibrium constant
k_s, k_{fs}	turbulence kinetic/scalar energy
k_r, k_{fr}	resolved turbulent kinetic/scalar fluctuation energy
k_{tot}, k_p	total/periodic component of turbulent kinetic energy
L_t	turbulence length scale
M_i	molecular weight of specie i

u, v	axial and transverse velocities
u_0, u_j	approach air and fuel-jet velocity
P, PDF	probability density function
P_F	cumulative probability of ignition
\dot{r}_{CO_2}	reaction rate of CO_2
R	resolved fluctuations
R_u	universal gas constant
Re_t	local turbulent Reynolds number
S_B	source term in reactedness equation
S_{ij}	resolvable strain tensor
Sc	Schmidt number
St	Strouhal number
$t_0 (= D/u_0)$	characteristic time
T	temperature
x_i	co-ordinate directions ($i = 1, 2$)
Y_i	mass concentration
$Y_{\text{CO}_2}^*$	normalized concentration of CO_2

Greek letters

δ_{ij}	Kronecker delta ($\delta_{ij} = 0$ for $i \neq j$; $\delta_{ij} = 1$ for $i = j$)
ε_f	dissipation rate of the scalar fluctuations
ν_t	eddy viscosity coefficient
ρ	density
σ_k	turbulent Prandtl number
τ_{ch}	chemical time scale
τ_e	turbulent/chemical exchange time
τ_{id}	turbulence/chemical ignition delay time
τ_{ij}, σ_{ij}	stresses
τ_k	Kolmogorov time scale
τ_t, τ_λ	time scales of turbulence
Δf_R	reaction zone width in f space
$\Delta, \Delta x, \Delta y$	characteristic mesh sizes
Σ_f	scalar scale

Operators

\dots'	turbulent (SGS) quantity
$\langle \dots \rangle$	Favre-resolved quantities
$\overline{\langle \dots \rangle}$	time-averaged value

Subscripts

A, a	air
ch	chemical
cr	critical

f	fuel
i	$i = 1, 2$ cylindrical co-ordinates
i, j	tensor notation
I	inert mixing gas state
L	lean
O	lower partial equilibrium boundary gas state
Q	any transitional gas state between states O and I
R	rich
s	subgrid scale, stoichiometric
t	turbulent flow

Superscripts

*	normalized value
---	------------------

REFERENCES

- Borghi R, Dupoirieux F, Zamuner B, Galzin F, Mantel T. Recent progress in the modeling of turbulent combusting flows. In *Experimental Heat Transfer, Fluid Mechanics and Thermodynamics*, Giot M, Mayinger F, Celata GP (eds). Edizioni ETS: Pisa, Italy, 1997; 2589–2602.
- Tolpadi AK, Zu IZ, Correa SH, Burrus DL. Coupled Lagrangian Monte Carlo PDF–CFD computation of gas turbine combustor flow fields with finite-rate chemistry. *Journal of Engineering Gas Turbines and Power* 1997; **119**: 519–526.
- Ravet F, Vernisch L. Modelling non-premixed turbulent combustion in aeronautical engines using PDF-Generator. AIAA Paper 1027, 36th Aerospace Sciences Meeting and Exhibition, Reno NV, 1998.
- Schefer RW, Namazian M, Kelly J. Velocity measurements in a turbulent nonpremixed bluff-body stabilized flows. *AIAA Journal* 1994; **32**(9): 1844–1851.
- Ercoftac Bulletin. First Aerodynamics and Steady State Combustion Chambers and Furnaces (ASCF-SIG) Workshop. Final Results, ERCOFTAC-SIG, October 1994. No. 25, June, 1995; 29–35.
- Roquemore WM, Tankin RS, Chin HH, Lottes AA. The role of vortex shedding in a bluff-body combustor. In *Experimental Measurements and Technology in Turbulent Reactive and Non-Reactive Flows*, vol. 66, So RMC, Roquemore WM, Whitelaw JH (eds). American Society of Mechanical Engineers, Applied Mechanics Division: New York, 1984; 68–72.
- Takahashi F, Schmoll WJ, Trump DD, Goss LP. Vortex-flame interactions and extinction in turbulent jet diffusion flames. 26th International Symposium on Combustion (Published by The Combustion Institute, Pittsburgh, USA), 1996; 145–152.
- Poinsot T, Veynante D, Trouve D, Reutsch GR. Turbulent flame propagation in partially premixed flames. Proceedings of the Summer Program, Center for Turbulence Research, Published by NASA Ames/Stanford University, Stanford, Connecticut, USA, 1996; 11–136.
- Obounou M, Gonzalez M, Borghi R. A Lagrangian model for predicting turbulent diffusion flames with chemical kinetic effects. 25th International Symposium on Combustion (Published by The Combustion Institute, Pittsburgh, USA), 1994; 1107–1113.
- Gran IR, Melaen MC, Magnussen BF. Numerical simulation of local extinction effects in turbulent combustor flows of CH₄ and air. 25th International Symposium on Combustion (Published by The Combustion Institute, Pittsburgh, USA), 1994; 1283–1291.
- Masri AR, Dibble RW, Barlow RS. The structure of turbulent non-premixed flames revealed by Raman–Rayleigh–LIF measurements. *Progress in Energy and Combustion Science* 1996; **22**: 307–362.
- Koutmos P. Simulations of turbulent methane jet diffusion flames with local extinction effects. *Fluid Dynamics Research* 1999a; **24**: 103–111.
- Koutmos P. A Damkohler number description of local extinction in turbulent methane jet diffusion flames. *FUEL* 1999b; **78**: 623–626.

14. Perin M, Namazian N, Kelly J, Schefer RW. Effects of confinement and blockage ratio on non-premixed turbulent bluff-body burner flames. Poster presented at the 23rd International Symposium on Combustion (Published by The Combustion Institute, Pittsburgh, USA), 1990; 60–63.
15. Menon S, Calhoon WH. Subgrid mixing and molecular transport modeling in a reacting shear layer. 26th International Symposium on Combustion (Published by The Combustion Institute, Pittsburgh, USA), 1996; 59–66.
16. Vernisch L, Poinso T. Direct numerical simulation of non-premixed turbulent flames. *Annual Review of Fluid Mechanics* 1998; **30**: 655–692.
17. Goutorbe T, Laurence D, Maupu V. An *a priori* test of an SGS tensor model including anisotropy and backscatter effects. In *Direct and Large Eddy Simulations I*, Voke PR, Kleiser L, Chollet JP (eds). Kluwer Academic: Dordrecht, 1994; 121–131.
18. Koutmos P, Mavridis C, Papailiou D. A study of turbulent diffusion flames formed by planar fuel injection into the wake formation region of a slender square cylinder. 26th International Symposium on Combustion (Published by The Combustion Institute, Pittsburgh, USA), 1996; 161–168.
19. Jimenez J, Linan A, Rogers MM, Higuera FJ. *A priori* testing of subgrid models for chemically reacting non-premixed turbulent shear-flows. Center for Turbulence Research. Proceedings of the Summer Program, Published by NASA Ames/Stanford University, Stanford, Connecticut, USA, 1996; 89–110.
20. Leonard BP. A stable and accurate convective modeling procedure based on quadratic upstream interpolation. *Computer Methods in Applied Mechanics and Engineering* 1979; **19**: 59–98.
21. Davis RW, Moore EF, Roquemore WM, Chen LD, Vilimpc V, Goss LP. Preliminary results of a numerical-experimental study of the dynamic structure of a buoyant jet diffusion flame. *Combustion and Flame* 1982; **83**: 263–270.
22. Akselvoll K, Moin P. Large-eddy simulation of turbulent confined coannular jets. *Journal of Fluid Mechanics* 1996; **315**: 387–411.
23. Van Driest ER. On turbulent flow near a wall. *Journal of Aeronautical Science* 1956; **23**: 1007–1015.
24. Koutmos P, Mavridis C, Papailiou D. A study of unsteady wake flows past a two-dimensional square cylinder with and without planar jet injection into the vortex formation region. *Applied Scientific Research* 1996; **55**: 187–210.
25. Nau M, Wolfert A, Maas U, Warnatz J. Application of a combined PDF/finite-volume scheme on turbulent CH₄ diffusion flames. *Ercoftac Bulletin* 1995; **26**: 22–26.
26. Neveu F, Corbin F, Trinite M, Perrin M. Simultaneous velocity and temperature measurements in a non-premixed bluff-body flame. *Ercoftac Bulletin* 1995; **26**: 11–16.